Self-Propulsion of Immersed Objects via Natural Convection

Matthieu J. Mercier,[1,*] Arezoo M. Ardekani,[2,3] Michael R. Allshouse,[1] Brian Doyle,[1] and Thomas Peacock[1]
[1]*ENDLab, Department of Mechanical Engineering, Massachusetts Institute of Technology, Cambridge, Massachusetts 02139, USA*
[2]*Aerospace and Mechanical Engineering, University of Notre Dame, Notre Dame, Indiana 46556, USA*
[3]*School of Mechanical Engineering, Purdue University, 585 Purdue Mall, West Lafayette, Indiana 47907, USA*
(Received 27 May 2013; published 21 May 2014)

Natural convection of a fluid due to a heated or cooled boundary has been studied within a myriad of different contexts due to the prevalence of the phenomenon in environmental and engineered systems. It has, however, hitherto gone unrecognized that boundary-induced natural convection can propel immersed objects. We experimentally investigate the motion of a wedge-shaped object, immersed within a two-layer fluid system, due to a heated surface. The wedge resides at the interface between the two fluid layers of different density, and its concomitant motion provides the first demonstration of the phenomenon of propulsion via boundary-induced natural convection. Established theoretical and numerical models are used to rationalize the propulsion speed by virtue of balancing the propulsion force against the appropriate drag force.

DOI: 10.1103/PhysRevLett.112.204501 PACS numbers: 47.55.P−, 47.15.−x, 47.85.−g

The phenomenon of natural convection generated by heated and cooled surfaces is ubiquitous. In engineering, for example, the effect is exploited to control transport and reactions in microfluidic devices [1] and in temperature control strategies for nuclear reactors [2] and buildings [3]. In geophysical systems, natural convection due to boundary cooling or heating is prevalent as anabatic and katabatic winds in valleys and over glaciers, respectively [4], and impacts the melting of icebergs [5]. Despite almost a century of research [6], although there have been a few studies of the motion of objects floating on the surface of [7], or immersed within [8], flows driven by natural convection, studies of boundary-induced natural convection have been restricted to systems with fixed boundaries [9]. Recently it has been demonstrated that a related class of boundary-layer flow, driven by molecular diffusion, can propel objects immersed in a fluid [10], albeit very slowly. Boundary-layer flows generated via natural convection are typically orders of magnitude stronger than their diffusive counterpart, and therefore have the potential to generate substantially faster propulsion speeds.

To investigate the concept of natural convection driven propulsion, a triangular wedge of length $\ell = 260$ mm, slope angle $\phi = 30°$ and width $w = 61$ mm was constructed and immersed in a two-layer fluid system, images of which are presented in Fig. 1(a). The dimensions of the wedge were chosen so that is was much narrower than the experimental tank, to limit the impact of sidewalls, and could accommodate an internal power supply and control electronics. A metal heating pad of length $\ell_h = 113.5$ mm and also 61 mm in width, flush-mounted in one of the sloping surfaces, was used to generate boundary layer convection. The pad was heated by a remotely activated 21 ± 1 W battery within the wedge. To isolate the wedge from surface tension effects that influence motion of an object floating at a free surface, its density was configured such that it was suspended within a two-layer stratification in an experimental tank 740 mm long, 510 mm wide, and 350 mm deep, with the base of the wedge level with the interface between the upper ($\rho = 1000$ kg m^{-3}) and lower ($\rho = 1100$ kg m^{-3}) fluid layers, lying 50 mm below the free surface [this two-layer arrangement caused a slight optical distortion of the appearance of the wedge when viewed from the side, evident in Fig. 1(a)].

The wedge was started from rest using a release procedure in which it initially settled within the confines of a cage of several vertical rods. Once the ambient disturbances generated by introducing the wedge into the tank had dissipated ($\sim$45 min) the cage was raised slowly, leaving the wedge drifting free in the quiescent stratification [its center located near the 140 mm tick in Fig. 1(a)]. As demonstrated by the data in Fig. 1(b), the unheated wedge remained essentially stationary for around 300 s (although there was some slight motion, on the order of 0.03 mm s^{-1}, due to unavoidable, weak ambient currents in such a large experimental tank), at which point the heating pad was remotely activated and motion commenced. Afterwards, the wedge was propelled a distance of $\sim$150 mm, attaining a maximum speed of $U \sim 0.6$ mm s^{-1}.

To rationalize the observed propulsion speed, we appeal to an established model of convection induced by a heated, two-dimensional, semi-infinite flat plate inclined at angle ϕ with respect to the horizontal in a homogenous ambient fluid of density $\rho = \rho_\infty$, temperature $T = T_\infty$, constant thermal expansivity β, thermal diffusivity α, thermal conductivity λ, and kinematic viscosity ν [11]. Provided the length of the heated surface greatly exceeds the characteristic distance, ℓ_t, for the boundary-layer flow to transition from horizontal to vertical-like behavior (for the wedge, $\ell_t \sim 1$ mm $\ll \ell_h \sim 100$ mm), a modified version of the

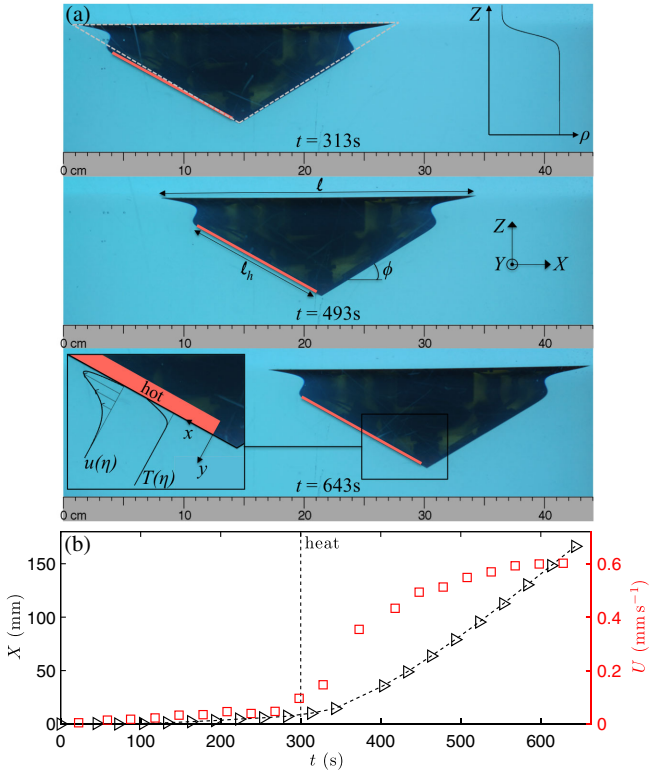

FIG. 1 (color online). (a) (top to bottom) A sequence of three images of the wedge moving in a two-layer stratification after the heated surface was activated (~300 s), the initial cage release is at $t = 0$ s. The apparent shape of the wedge is distorted slightly by the vertically varying optical properties of the stratification (top right), and the active heating pad is indicated in red. (lower left) A schematic of the velocity and temperature profiles induced by the heated surface. (b) Displacement (▷) and speed (□) of the wedge as a function of time.

similarity solution for a vertical boundary can be used for any slope angle [12].

Defining x and y to be coordinates parallel and perpendicular to the heated surface, respectively, with the origin at the leading edge, and u and v to be the corresponding velocity components [see inset Fig. 1(a)], the similarity parameter $\eta = \gamma(x)y/x$ is introduced, along with the rescaled variables [11],

$$f(\eta) = \frac{\psi(x,y)}{5\nu\gamma(x)}, \qquad \theta(\eta) = \frac{\lambda\gamma(x)(T - T_\infty)}{qx}, \tag{1}$$

where $\psi(x,y)$ is the stream function such that $(u,v) = (\partial\psi/\partial y, -\partial\psi/\partial x)$, $\gamma(x) = [\mathrm{Gr}(x)\sin\phi/5]^{1/5}$, $\mathrm{Gr}(x) = g\beta q x^4/\lambda\nu^2$ is the local Grashoff number at position x, q is the boundary heat flux, and g is gravity. The resulting coupled boundary layer equations are

$$f''' + 4ff'' - 3f'^2 + \theta = 0, \tag{2}$$

$$\frac{1}{\mathrm{Pr}}\theta'' + 4f\theta' - f'\theta = 0, \tag{3}$$

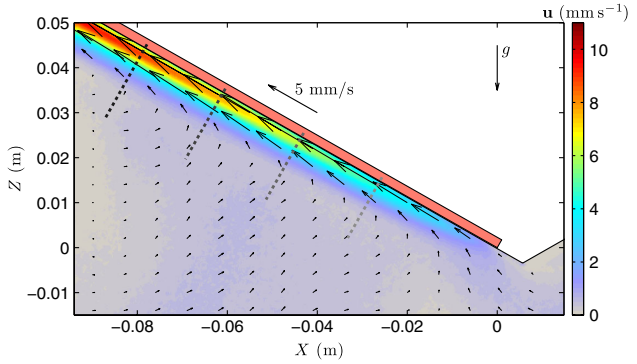

FIG. 2 (color online). The experimental PIV velocity field, magnitude (color map), and direction (arrows), in the vicinity of the heated surface of the stationary wedge for a 21 ± 1 W battery. The rectangular shaded region within the wedge indicates the heated surface, similarly to Fig. 1, and the dashed gray lines are transects along which experimental data are compared with theory and numerics in Fig. 3.

where $\mathrm{Pr} = \nu/\alpha$ is the Prandtl number. No-slip and constant heat flux are assumed at the surface of the heated plate, and $u = v = 0$ and $T = T_\infty$ as $y \to \infty$, in which case the rescaled boundary conditions are $f(0) = f'(0) = 0$, and $\theta'(0) = -1$ and $f' = \theta = 0$ as $\eta \to \infty$. For a given value of Pr, the similarity solutions for f and θ must be determined numerically.

To validate the applicability of the theoretical model, we used particle image velocimetry (PIV) to experimentally determine the velocity field induced by the heated surface with the wedge held stationary. Figure 2 presents the velocity field in the central vertical plane of the wedge. The boundary layer flow achieved a steady state 300 s after heating commenced and the PIV data presented is an average over a 30 s time window around 600 s after the battery was activated. Away from the boundary, a weak recirculation is visible, due to entrainment by the boundary layer flow. There was a $\lesssim$20% weakening of the flow velocity magnitude for vertical planes 20 mm either side of the central plane, and thus only a modest departure from two dimensionality for the experiments. It was not possible, however, to experimentally resolve the structure of the ~3 mm thick thermal boundary layer using the available technology. In addition to the PIV studies, we also performed a two-dimensional, two-layer numerical simulation for a cross section of the experiment using COMSOL.

Figure 3 presents a comparison of theoretical, experimental, and numerical velocity profiles for the transects indicated in Fig. 2. For each transect, the velocity component along the wall is transformed according to Eq. (1) and scaled by the local maximum velocity $u^*(x) = [5\nu\gamma(x)^2 f'^*/x]$, f'^* being the maximum of $f'(\eta)$, and the profiles are plotted as a function of the similarity variable η. In addition to the velocity profiles, theoretical and numerical rescaled temperature profiles for the same transects are presented (in red) in Fig. 3. The values used for the

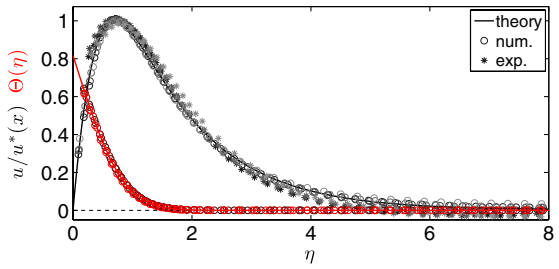

FIG. 3 (color online). Comparison of experimental (*) and numerical (∘) data with the analytical model, using $\mathrm{Pr} = 9.1$, for the velocity (black, with a maximum near $\eta = 1$) and temperature (red, monotonically decreasing from 0.8 to 0) profiles extracted along the four transects indicated in Fig. 2. The intensity of the color (gray or red) for experimental and numerical points is an indication of the transect considered in Fig. 2.

physical parameters in the theoretical and numerical models are: $\beta = 2.07 \times 10^{-4}\ \mathrm{K}^{-1}$, $\lambda = 0.58\ \mathrm{W\,m^{-1}\,K^{-1}}$, $T_\infty = 20°\mathrm{C}$, $\rho_\infty = 1100\ \mathrm{kg\,m^{-3}}$, $\alpha = 1.26 \times 10^{-7}\ \mathrm{m^2 s^{-1}}$, and $\nu = 1.14 \times 10^{-6}\ \mathrm{m^2 s^{-1}}$, the latter two setting $\mathrm{Pr} = 9.1$. Although temperature influences the value of many of these parameters, within the context of this first order model we use these constant values. Setting the appropriate value of the constant boundary heat flux is not quite as straightforward as simply dividing the power supplied (21 ± 1 W) by the surface area of the heating plate (113.5 mm × 61 mm), since infrared thermal imaging in air revealed that the experimental surface was preferentially heated in the center, with $\lesssim$10% variation of the surface temperature away from the center of the plate. The best match between the experimental boundary layer flow in Fig. 3 and the analytical profile was for an effective heat flux $q = 5000\ \mathrm{W\,m^{-2}}$, which is of the same order as the value of $3033 \pm 144\ \mathrm{W\,m^{-2}}$ if the heat flux were uniformly distributed; this empirical enhancement factor of $5/3$ gave very good agreement for all the velocity profiles and heat fluxes investigated.

Overall there is close agreement for all velocity profiles in Fig. 3, demonstrating that a well-defined and understood boundary layer flow was established. There is similarly close agreement between theory and numerics for the corresponding temperature profiles, confirming the associated structure of the thermal boundary layer. We note that the characteristic Rayleigh number for this system $\mathrm{Ra}(\ell) = \mathrm{Pr}\,\mathrm{Gr}(\ell) \leq 10^{10}$; hence, the flow is laminar, not turbulent [13,14].

We will now use the validated analytical and numerical models to estimate the horizontal propulsion force, F_x, acting on the wedge. In so doing, we note that for the experimental parameter values, the characteristic boundary layer velocity (~5 mm s^{-1}) is an order of magnitude greater than the propulsion speed (~0.6 mm s^{-1}), and so it is reasonable to assume that the boundary layer flow persists on the moving wedge. For a two-dimensional boundary layer across the width of the wedge, the net force as a result of pressure and viscous drag is

$$F_x = w \int_0^{\ell_h} \left[p(x,0) \sin\phi - \rho_\infty \nu \frac{\partial u}{\partial y}(x,0) \cos\phi \right] dx, \quad (4)$$

where we have neglected temperature effects for the properties of the fluid.

In terms of the scaled variables

$$F_x = \frac{25}{7} \frac{w}{\ell_h} \rho_\infty \nu^2 \mathrm{Gr}_\star^{3/5} \cos\phi \left[\int_0^\infty \theta(\eta) d\eta - f''(0) \right], \quad (5)$$

where $\mathrm{Gr}_\star = \mathrm{Gr}(\ell_h) \sin\phi/5$, and the expression in parentheses is found to vary like $\mathrm{Pr}^{-9/10}$ over the range $10^{-2} < \mathrm{Pr} < 10^3$. Figure 4(a) presents a comparison of theoretical and numerical results for the propulsion force on the wedge as a function of the heat flux using the previously

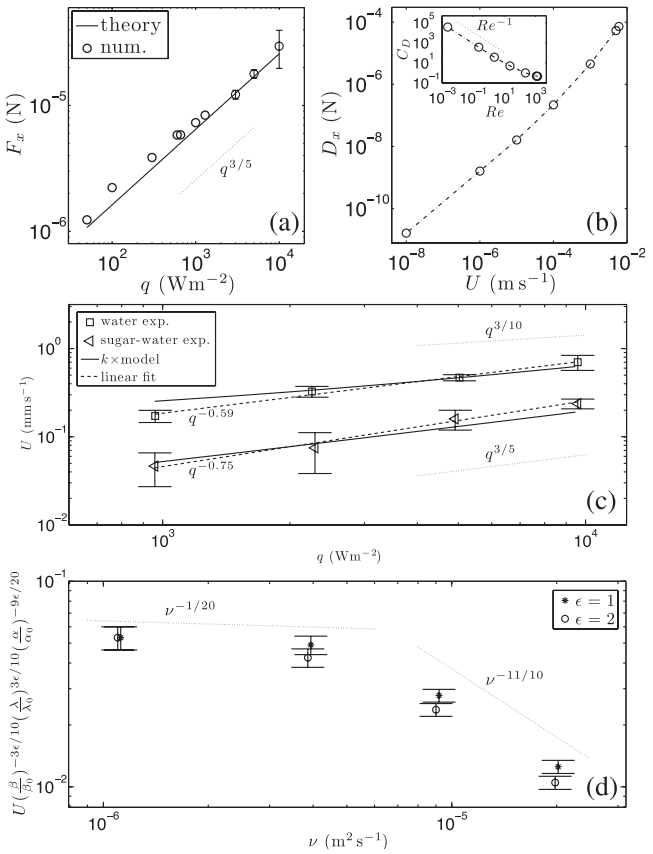

FIG. 4. (a) Theoretical (−) and numerical calculations (∘) of the propulsion force as a function of heat flux, for the physical parameters listed in the text. (b) Numerical results for the drag on a fixed 3D wedge as a function of the flow velocity U; (inset) same data in dimensionless form, i.e., he drag coefficient as a function of the Reynolds number. (c) Propulsion speed as a function of the power input for experiments in water (□) and sugar water (◁), linear fits to the experimental data (−−) and the theoretical prediction (−) rescaled by a factor $k = 1/5$. (d) Evolution of the rescaled experimental propulsion speed, in mm s^{-1}, as a function of the kinematic viscosity for an effective power input $q = 5000\ \mathrm{W\,m^{-2}}$.

stated values for the other physical parameters, the numerical results confirming the theoretical prediction $F_x \propto q^{3/5}$.

The thrust force generated by natural convection causes the wedge to accelerate from rest and consequently experience a drag force, D_x, that resists its motion, the nature of which depends on the Reynolds number, $\mathrm{Re} = U\ell/\nu$. To estimate drag as a function of propulsion speed, a three-dimensional COMSOL simulation was used to calculate the net force on the wedge (without a heated surface) for oncoming flow over the range of speeds $10^{-8}\ \mathrm{m\,s^{-1}} < U < 10^{-2}\ \mathrm{m\,s^{-1}}$. The results are presented in Fig. 4(b), the inset showing the drag coefficient of the wedge, $C_D = 2D_x/\rho_\infty A U^2$, where A is the cross sectional area in the direction of motion, as a function of the Reynolds number. For $U < 10^{-4}\ \mathrm{m\,s^{-1}}$ and $\mathrm{Re} < 10$, it is found that $C_D \propto \mathrm{Re}^{-1}$, corresponding to predominantly viscous drag. For the range $10^{-4}\ \mathrm{m\,s^{-1}} < U < 10^{-2}\ \mathrm{m\,s^{-1}}$, and $\mathrm{Re} > 10$, the system transitions from viscous toward inertial drag, where C_D varies little with Re. As an additional check, we investigated the potential influence on the drag force of natural convection over the heated rear surface of the wedge. Several three-dimensional COMSOL investigations for a range of heat fluxes revealed no noteworthy change.

For a given set of parameters, matching the data presented in Figs. 4(a) and 4(b) gives a prediction for the wedge propulsion speed ["model" in Fig. 4(c)]. Additionally, and for simplicity using ℓ as the length scale for both the wedge and the heated surface, balancing the propulsion force, Eq. (5), against a viscous drag force leads to $U \propto q^{3/5}\ell^{7/5}\beta^{3/5}\lambda^{-3/5}\alpha^{9/10}\nu^{-11/10}$ at low Reynolds numbers (i.e., $D_x \propto \rho\nu U\ell$), whereas at high Reynolds number (i.e., $D_x \propto \rho U^2\ell^2$) one finds $U \propto q^{3/10}\ell^{1/5}\beta^{3/10}\lambda^{-3/10}\alpha^{9/20}\nu^{-1/20}$. The most practical parameters to vary in a lab experiment are the heat flux and the viscosity.

We first ran a series of experiments using four different batteries covering the effective heat flux range $950\ \mathrm{W\,m^{-2}} < q < 9490\ \mathrm{W\,m^{-2}}$ for the cases of water and a sugar-water mixture; for the theoretical and numerical calculations, the physical parameters previously listed for water were used, whereas for the sugar-water solution we measured the kinematic viscosity ($2.0 \times 10^{-5}\ \mathrm{m^2\,s^{-1}}$) and obtained other parameter values (e.g., $\mathrm{Pr} = 140$) from tabulated data [15]. A comparison of the experimental data and model predictions is presented in Fig. 4(c). For the sugar-water experiments ($0.7 < \mathrm{Re} < 4$), a linear fit to the data has a slope of 0.75 ± 0.18, whereas for the water experiments ($36 < \mathrm{Re} < 150$) the experimental slope is noticeably shallower at 0.59 ± 0.18. These results are commensurate with the theoretical power law that transitions from 3/5 to 3/10 as the Reynolds number increases, although the predicted speeds exceed experimental values by a factor ~5. This discrepancy is reasonable given the first-order nature of the model and several practical reasons can justify this overestimate, leading candidates being the finite size of the experimental tank enhancing drag, inhomogeneous surface heating, and the three dimensionality of the experimental system.

Experiments were performed for $q = 5000\ \mathrm{W\,m^{-2}}$ using a range of sugar-water solutions (0%, 33%, 47%, and 57% by mass) corresponding to viscosities in the range $1.1 \times 10^{-6}\ \mathrm{m^2\,s^{-1}} \leq \nu \leq 2.0 \times 10^{-5}\ \mathrm{m^2\,s^{-1}}$; the goal being to investigate the impact of kinematic viscosity on the propulsion speed that is expected to display a clear transition from a viscous regime ($U \propto \nu^{-11/10}$) to an inertial regime ($U \propto \nu^{-1/20}$) as the Reynolds number increases through unity. The results, presented in Fig. 4(d), cover the range $1.9 < \mathrm{Re} < 125$. Since changes in sugar content also impact values of the other physical parameters (e.g., ~20% and ~40% decrease for α and λ respectively; ~40% increase for β), this is accounted for by rescaling the measured speeds by the factor $(\beta/\beta_0)^{-3\epsilon/10}(\lambda/\lambda_0)^{3\epsilon/10}(\alpha/\alpha_0)^{-9\epsilon/20}$, with $\epsilon = 1$ and $\epsilon = 2$ corresponding to the appropriate scaling for the inertial and viscous regimes, respectively, and β_0, λ_0, and α_0 being the parameter values for water. A distinct change in the functional dependence on viscosity is observed throughout the transitional range of Reynolds number covered by these experiments, consistent with the theoretically predicted scalings.

In conclusion, we have presented the first demonstration of the phenomenon of propulsion via boundary-induced natural convection. The magnitude of the propulsion speed, and its dependence on surface heat flux and kinematic viscosity are reasonably predicted using a first-order approach based on existing models for thermal boundary layer flow and drag. For the water-based environments, physical scale, and shape we have studied the propulsion speed is on the order of $1\ \mathrm{mm\,s^{-1}}$. Although our work focuses on the laminar regime, it would be of interest to extend these results to the turbulent natural convection regime, with $\mathrm{Ra}(\ell) \geq 10^{10}$. Indeed, studies have shown that the mean velocity and temperature boundary layer profiles are similar to the laminar case except for the exponents in the power law for Gr_ℓ [16,17], suggesting the possibility of propulsion for this regime too. Given the ubiquity of boundary-induced natural convection in engineering and natural processes, there is potentially widespread application to topics as diverse as bioengineering, microfluidics, and geosciences. Possible research directions could be to investigate the impact of the effect on the drift of icebergs [18] or the transport of suspended material within magma chambers [19]. Because of the dependence of the effect on a wide range of physical parameters associated with the fluid and the object, there are untold physical and biological settings for which this phenomenon might warrant further investigation. Quite simply, any scenario in which an immersed object has either a different temperature than the surrounding fluid, or has an internal heat source or sink, is a candidate for consideration.

We thank Professor S. Sarma for use of an IR camera, A. Gallant for fabrication of the experimental wedge, and anonymous referees for their constructive comments.

*Present address: IMFT (Institut de Mécanique des Fluides de Toulouse), Allée Camille Soula, F-31400 Toulouse, France.

[1] M. Krishnan, N. Agrawal, M. A. Burns, and V. M. Ugaz, Ann. Chem. **76**, 6254 (2004).
[2] M. Bazargan, D. Fraser, and V. Chatoorgan, J. Heat Transfer **127**, 897 (2005).
[3] P. F. Linden, Annu. Rev. Fluid Mech. **31**, 201 (1999).
[4] J. Oelemans and B. Grisogono, Tellus A **54**, 440 (2002).
[5] H. E. Huppert and J. S. Turner, Nature (London) **271**, 46 (1978).
[6] A. Leveque, Ph.D. thesis, Faculté des Sciences de Paris, 1928, http://www.worldcat.org/oclc/459642198.
[7] J. Zhang and A. Libchaber, Phys. Rev. Lett. **84**, 4361 (2000).
[8] J. A. Whitehead, Phys. Earth Planet. Inter. **5**, 199 (1972).
[9] E. Chassignet, C. Cenedese, and J. Verron, *Buoyancy-Driven Flows* (Cambridge University Press, Cambridge, England, 2012).
[10] M. R. Allshouse, M. F. Barad, and T. Peacock, Nat. Phys. **6**, 516 (2010).
[11] T. S. Chen, H. C. Tien, and B. F. Armaly, Int. J. Heat Mass Transfer **29**, 1465 (1986).
[12] A. Umemura and C. K. Law, J. Fluid Mech. **219**, 571 (1990).
[13] Y. Jaluria and B. Gebhart, Int. J. Heat Mass Transfer **20**, 434 (1977).
[14] V. L. Vitharana and P. S. Lykoudis, J. Heat Transfer **116**, 633 (1994).
[15] F. Á. Mohos, *Confectionery and Chocolate Engineering: Principles and Applications* (Wiley-Blackwell, Oxford, 2010).
[16] T. Tsuji and Y. Nagano, Exp. Therm. Fluid. Sci. **2**, 208 (1989).
[17] M. Z. Abedin, T. Tsuji, and Y. Hattori, Int. J. Heat Mass Transfer **52**, 4525 (2009).
[18] D. G. Mountain, Cold Reg. Sci. Technol. **1**, 273 (1980).
[19] F. Blanchette, T. Peacock, and J. W. M. Bush, Geophys. Res. Lett. **31**, L05611 (2004).